Determination of Fluorescence Density Profiles of Langmuir–Blodgett-Deposited Films by Analysis of Variable-Angle Fluorescence Data Curves

Peter A. Suci* and William M. Reichert†

Department of Bioengineering and Center for Biopolymers at Interfaces, University of Utah, Salt Lake City, Utah 84112

Received December 8, 1987. In Final Form: April 7, 1988

By use of the method of Langmuir–Blodgett deposition thin films with three different spatial distributions of fluorophores were constructed. The films were deposited on the flat surface of a sapphire hemicylindrical prism. Each film had a thickness of 55.44 nm. The spatial distribution of each film type was in the form of a rectangular fluorescence density profile: monolayers containing fluorophores were confined to be within a specific range in terms of distance from the prism/film interface. Rectangular profiles can be characterized by the parameters of amplitude, position (center), and width. Light from an argon ion laser (488-nm line), which was incident on the prism/film interface, was used to excite fluorescence in each of the film types. Fluorescence was collected as a function of both incident and observation angles. It was found that variable-angle fluorescence data curves taken from the films could be used to predict an approximate position of each rectangular profile. Based on reduced χ^2 values predictions of position made from variable incident angle curves were more reliable than those made from variable observation angle curves. The effect of an index matching fluid, placed adjacent to the film, was to cause the position to be underestimated. An analysis of data curves did not result in a reliable estimation of the parameter of width. Results from simulated data indicate that data curves could support fitting of all three parameters (amplitude, position, and width) at quantum noise levels comparable to the noise levels of the actual data. Therefore, the failure of the analysis to predict the width parameter is attributed to a distortion in the data curves rather than the effect of quantum noise from photon collection. Possible improvements in the apparatus which may reduce this distortion are discussed.

Introduction

The purpose of this study was to provide information relevant to the evaluation and further development of a relatively new fluorescence technique. This technique can yield parameters of the fluorescence density profile of a thin dielectric film. A fluorescence density profile is the average density of fluorophores with respect to distance away from the substrate/film interface into the film. The Langmuir–Blodgett (L–B) technique has been utilized in this study in order to construct films having model fluorescence density profiles. Our research effort has been aimed toward testing the potential of the technique for predicting the shape of profiles in films having a thickness comparable to films of interest in biomedical studies.

Various optical techniques have been used to characterize thin films in biomedically related studies.[1-5] Optical analysis of dielectric thin films is especially advantageous when the films are biological material because light in the infrared, visible, or ultraviolet range is relatively nondestructive to most molecules of interest, and the information can be gathered under ambient conditions. In general, optical techniques offer the possibility of monitoring dynamic processes. Adsorbed protein layers (an important determinant of biocompatibility) and covalently bound biopolymers (the active element in current sensor designs) are both essentially thin dielectric films. A fluorescence density profile of such films could be used to determine a layer thickness or to verify a predicted orientational preference on a surface.

Information about fluorescence density profiles of thin films can be obtained via an analysis of variable-angle fluorescence data curves.[6,7] In the simplest experimental setup, the film is deposited directly on a high-index transparent prism. A collimated light source is directed at the prism/film interface such that it intersects the interface at a specific incident angle (Figure 1a). Some of the incident light penetrates into the film and excites fluorescence. The fluorescence that back-couples through the prism is measured in the plane of incidence at an angle, which will be referred to, in this paper, as the observation angle. A variable incident angle fluorescence data curve is obtained by measuring fluorescence at a fixed observation angle for incident angles which range from normal to grazing. Its counterpart, a variable observation angle fluorescence data curve, is obtained by measuring fluorescence at a fixed incident angle for observation angles which range from the normal to grazing (Figure 1b). Both incident and observation angle fluorescence data curves can be used to obtain information about the fluorescence density profile of a thin film.

An analysis of variable angle fluorescence data curves has been used to determine the thickness of depletion layers of polymer solutions[8-10] and to estimate the concentration and emission dipole orientation of adsorbed dye molecules.[11] Recently, variable incident angle data taken

* Author to whom correspondence should be sent.
† Current address: Dept. of Biomedical Engineering, Duke University, Durham, NC 27706.

(1) Cuypers, P. A.; Hermens, W. Th.; Hemker, H. C. *Anal. Biochem.* **1978**, *84*, 56.
(2) Corsel, J. W.; Willems, G. M.; Kop, J. M. M.; Cuypers, P. A.; Hermens, W. Th. *J. Colloid Interface Sci.* **1986**, *3*, 544.
(3) Gendreau, R. M. *Spectroscopy in the Biomedical Sciences*; Gendreau, R. M., Ed.; CRC: Boca Raton, FL, 1986.
(4) Van Wagenen, R. A.; Rockhold, S. A.; Andrade, J. D. *Adv. Chem. Ser.* **1982**, *199*, 351.
(5) Rockhold, S. A.; Quinn, R. D.; Van Wagenen, R. A.; Andrade, J. D.; Reichert, W. M. *J. Electroanal. Chem.* **1983**, *150*, 261.
(6) Thompson, N. L.; Burghardt, T. P. *Biophys. Chem.* **1986**, *25*, 91.
(7) Hellen, E. H.; Axelrod, D. *Opt. Soc. Am. B* **1986**, *4*, 337.
(8) Allain, C.; Ausserre, D.; Rondelez, F. *Phys. Rev. Lett.* **1982**, *49*, 1694.
(9) Ausserre, D.; Hervet, H.; Rondelez, F. *Phys. Rev. Lett.* **1985**, *54*, 1948.
(10) Ausserre, D.; Hervet, H.; Rondelez, F. *Macromolecules* **1986**, *19*, 85.
(11) Fattinger, Ch.; Honegger, F.; Lukosz, W. *Helv. Phys. Acta* **1986**, *59*, 1079.

0743-7463/88/2404-1131$01.50/0

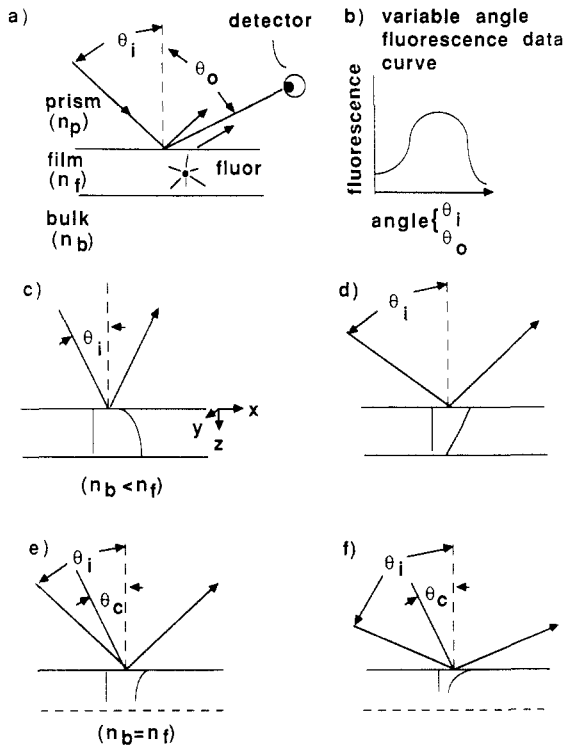

Figure 1. (a) General optical configuration showing incident (θ_i) and observation (θ_o) angles. (b) Variable-angle fluorescence data curve is obtained by varying either the incident or observation angle from normal to grazing. (c) An interference pattern, having a distinct intensity distribution, is produced in the film at all angles (0–90°) when $n_f > n_b$. (d) The intensity distribution of the field within the film can be manipulated by changing the incident angle. (e) Schematic representation of evanescent wave produced by total reflection of incident light beam with $n_f = n_b$. (f) Penetration depth decreases as incident angle (θ_i) is increased beyond the critical angle (θ_c).

from a polymer film deposited on a sapphire prism were resolved into fluorescence lifetime components of the film and bulk fluorophores.[12] The technique has been used, with tentative success, to estimate the thickness of adsorbed protein films. In these experiments it was found that the general shapes of variable-angle fluorescence data curves obtained from adsorbed layers of fluorescently labeled Immunoglobulin (FITC-IgG) conformed to expectation.[13,14] However, parameters of layer thickness and protein concentration obtained from a least-squares fit of a simple theoretical model to the data curves were inconsistent with expectation. The difficulty with using biological materials such as adsorbed protein layers to test the technique is that not only are the numerical methods relatively difficult but the interfaces are not well characterized. To a large extent, the L–B technique overcomes this latter problem, while allowing construction of fluorescence density profiles of a biomedically relevant scale.

In this paper we present variable-angle fluorescence data curves from three fluorescence density profiles constructed in the L–B trough. The L–B deposition method lends itself to construction of "rectangular" fluorescence density profiles in which the fluorophores are all contained in

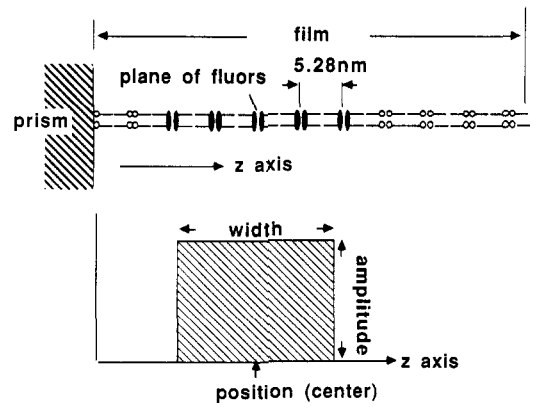

Figure 2. (Top) Schematic representation of construction of rectangular fluorescence density profiles using L–B deposition on the flat surface of the hemicylindrical prism. Solid ellipses represent the head groups of a cyanine dye (Figure 4), which are the fluorophores. Open circles represent arachidic acid (nonfluorescent) head groups. Long hydrocarbon chains are represented as lines. The dye head groups are, in actuality, incorporated into an acid head group matrix. (Bottom) The profile is represented graphically.

parallel planes that are at distances from the prism/film interface within a specific range (Figure 2). An ideal rectangular profile can be described completely by three parameters: amplitude, position (or center), and width. In all cases the film in which the planes of fluorophores were contained was deposited on the flat surface of a sapphire hemicylindrical prism. Each film was 55.44 nm thick. Variable-angle data curves were obtained from films in which the "bulk" material was air and from the same films in which the bulk material was a fluid of nearly the same refractive index as the film.

Theory

Angular Dependence of the Light Intensity Distribution in the Film. As shown in Figure 1a, light is incident on the planer interface between the high index prism and the film. Consider a thin film with a refractive index different from that of the bulk adjoining media. Light penetrating through the prism/film interface produces an interference pattern with a distinct intensity distribution in the film at all incident angles from normal to grazing (Figure 1c). Variation of the incident angle changes the distribution of energy in the film in terms of its magnitude in the z direction (Figure 1c,d). A fluorophore located in the film will fluoresce in proportion to the intensity of the electric field at that location. Theoretically, the curve obtained by measuring fluorescence emission for various incident angles (a variable incident angle fluorescence data curve) should have a distinct shape which depends, in part, upon the position of the fluorophore (with respect to distance from the prism/film interface).

If the refractive index of the bulk material is the same as that of the film, the distribution of energy is uniform throughout the film for incident angles less than the critical angle for the prism/film interface. Therefore, at these angles, the variable incident angle curve contains no fluorophore positional information. However, beyond the critical angle the intensity distribution is nonuniform and can be manipulated. At these angles an evanescent wave penetrates into the film. The evanescent wave is an electromagnetic field with an intensity which exponentially decays as it penetrates from the prism/film interface into the film and finally into the bulk material (Figure 1e). The exponential decay rate (or inverse penetration depth) of

(12) Masuhara, H.; Tamai, N.; Yamazaki, I. *J. Phys. Chem.* **1986**, *90*, 5830.
(13) Reichert, W. M.; Suci, P. A.; Ives, J. T.; Andrade, J. D. *Appl. Spectrosc.* **1987**, *41*, 503.
(14) Suci, P. A. "Variable Angle Total Internal Reflection Fluorescence"; Masters Thesis, Department of Bioengineering, University of Utah, 1985.

the evanescent wave can be varied by manipulating the incident angle (Figure 1e,f).

The theory for calculating the energy distribution within a thin film caused by incidence of a monochromatic plane wave is well-known.[15] The form of the specific expression which is presented here has been elaborated on elsewhere.[16] Only perpendicular polarized (TE) incident light is considered. At this polarization only the ordinary wave is propagated through the film, which is uniaxially birefringent.[17] The film is assumed to be bounded on one surface by a prism and on the other surface by some bulk material which is for practical purposes infinite in extent (Figure 1a). The following subscript notation will be used: p for the prism, f for the film, b for the bulk medium (air or high-index fluid), i for incident, and o for observation. Figure 1c indicates the coordinate system orientation.

Transmission angles, θ_f and θ_b, of rays entering the film and bulk material can be written in terms of the incident angle (θ_i) by employing Snell's law:

$$\theta_f = \sin^{-1}[(n_p/n_f)\sin\theta_i] \qquad (1)$$

$$\theta_b = \sin^{-1}[(n_p/n_b)\sin\theta_i]$$

where n_p, n_f, and n_b are the refractive indices of, respectively, the prism, the film, and the bulk material. By convention let

$$p_{sub} = n_{sub}\cos\theta_{sub} \qquad (2)$$

where the subscript, sub, can be p, f, or b.

The expression for energy at a location within the film ($I(x,y,z)$) can be written as a product of the interfacial intensity ($I_0(x,y)$) at a point on the prism/film interface and a term which is functionally dependent on distance (z) from the prism/film interface into the film:

$$I(x,y,z) = I_0(x,y)|\tau_f \exp(ik_0p_fz) + \tau_r \exp(-ik_0p_fz)|^2 \qquad (3)$$

The product (k_0p_f) is the z-component of the propagation vector of the waves within the film, where

$$k_0 = 2\pi/\lambda_i \qquad (4)$$

The convention of an implicit $\exp(-i\omega t)$ time dependence has been adopted.[18] The terms τ_f and τ_r can be written in terms of the reflection coefficient (r) of the film:

$$\tau_f = [(1 + r) + (p_p/p_f)(1 - r)]/2 \qquad (5)$$

$$\tau_r = [(1 + r) - (p_p/p_f)(1 - r)]/2$$

The reflection coefficient of the film (r) can be expressed in terms of the standard Fresnel reflection coefficients for a single prism/film and film/bulk interface (r_{pf} and r_{fb}, respectively):

$$r = [r_{pf} + r_{fa}\exp(2ik_0p_fd)]/[1 + r_{pf}r_{fa}\exp(2ik_0p_fd)] \qquad (6)$$

For TE light, the Fresnel reflection coefficients are

$$r_{pf} = (p_p - p_f)/(p_p + p_f) \qquad (7)$$

$$r_{fb} = (p_f - p_b)/(p_f + p_b)$$

The intensity in the film ($I(x,y,z)$) is thus dependent on the intensity of the incident radiation and a term which is functionally dependent on the experimentally known parameters of incident angle (θ_i) of the light beam, the free space wavelength of incident (excitation) light (λ_i), the refractive indices of the prism (n_p), the film (n_f), and the bulk material (n_b), the thickness of the film (d), as well as the distance (z) from the prism/film interface. Of these parameters the incident angle (θ_i) and the distance (z) are most pertinent to the analysis which follows. In order to simplify further discussion let

$$T(\theta_i,z) = |\tau_f \exp(ik_0p_fz) + \tau_r \exp(-ik_0p_fz)|^2 \qquad (8)$$

Angular Distribution of Fluorescence from a Single Fluorophore. The fluorophore emission pattern is distorted by each dielectric interface at which a refractive index mismatch occurs. The effect of this distortion depends, in part, upon the distance that the fluorophore is located from that interface. Therefore, the resulting angular pattern of fluorescence emission which is observed through the prism (a variable observation angle fluorescence data curve) contains fluorophore positional information. The significance of this is that variable observation angle fluorescence data curves can be used in lieu of variable incident angle fluorescence data curves for the purpose of obtaining fluorescence density profile information.

Fluorescence is observed in the plane of incidence in our experiments. The observation angle (θ_o) is defined as the angular position of the detector with respect to a normal to the interface (Figure 1a). Only fluorescence restricted to the perpendicular polarized (TE) component is considered in this discussion. At this polarization, one is essentially only observing fluorescence emission patterns from components of dipoles oriented perpendicular to the plane of incidence or along the y axis (Figure 1c).[7,19]

The quantity of the TE component of fluorescence ($F(\theta_i,\theta_o)$), detected at a particular incident (θ_i) and observation angle (θ_o), from a fluorophore located at a distance z from the prism/film interface can be determined by employing a principle of reciprocity.[16,20,21] Specifically

$$F(\theta_i,\theta_o) = P\,Q(z)\,I_0(x,y)\,T(\theta_i,z)\,T(\theta_o,z) \qquad (9)$$

where the term P is a proportionality constant. The term $T(\theta_o,z)$ in eq 9 is algebraically identical with the term $T(\theta_i,z)$ (which is defined in eq 8) with substitution of θ_o and λ_o for θ_i and λ_i. This last statement defines what we mean by reciprocity in this paper. Empirically, eq 9 has been shown to correctly predict the angular dependence of the TE fluorophore emission pattern from a single dye-containing monolayer for a quartz prism/L-B film/air interface configuration.[16] The term $T(\theta_o,z)$ can also be shown to be algebraically identical with the term $T(\theta_i,z)$ from theoretical considerations.[19] The term $Q(z)$ is a quantum yield term which will be discussed below. It is not the same as the fluorescence quantum yield, which is assumed to possess no distance dependence.

Angular Dependence of Fluorescence from a Spatial Distribution of Fluorophores. A fluorescence density profile ($\rho(z)$) is the average density of fluorophores contained in planes parallel to the prism/film interface with respect to the distance (z) from that interface. The angular dependence of fluorescence which should be obtained from a single plane of fluorophores located within the film at a distance (z) from the prism/film interface can be described by two equations.[16] The angular dependence on incident angle (with fixed observation angle) is

(15) Born, M.; Wolf, E. *Principles of Optics*; Pergamon: Oxford, 1980; p 55.
(16) Suci, P. A.; Reichert, W. M. *Appl. Spectrosc.* **1987**, *42*, 120.
(17) Drexhage, K. H. In *Progress in Optics*; Wolf, E., Ed.; North-Holland: New York, 1974; Vol. 7, p 164.
(18) Hansen, W. N. *J. Opt. Soc. Am.* **1968**, *58*, 380.
(19) Suci, P. A. Ph.D. Dissertation, University of Utah, in preparation, 1988.
(20) Carniglia, C. K.; Mandel, L.; Drexhage, K. H. *J. Opt. Soc. Am.* **1972**, *62*, 479.
(21) Lee, E.-H.; Benner, R. E.; Fenn, J. B.; Chang, R. K. *Appl. Opt.* **1979**, *18*, 862.

$$F_i(\theta_i;z) = A\ Q(z)\ G_i(\theta_i;z) \quad (10)$$

where

$$G_i(\theta_i;z) = (1/\cos\theta_i)\ T(\theta_i,z)$$

The observation angle dependence (at fixed incident angle) is

$$F_o(\theta_o;z) = A\ Q(z)\ G_o(\theta_o;z) \quad (11)$$

where

$$G_o(\theta_o;z) = T(\theta_o,z)$$

These expressions have been derived for our specific apparatus. The distance z has been included parenthetically as an independent variable of the expressions G_i and G_o in order to help clarify a point which is made below. The redefinition in terms of the expressions G_i and G_o is done for notational convenience. The amplitude (A) includes terms, such as incident light intensity and absorption and collection efficiency, which have no functionality with respect to the angle being varied or with respect to the distance z. The $1/\cos\theta_i$ term that appears in eq 10 results from the variation of the area of illumination with incident angle. It is an approximation based upon an estimation of the integral of a Gaussian intensity distribution over the prism/film interfacial plane.[16] An estimation of the small (less than 0.1%) error involved in the approximation, for the our particular experimental design, is discussed elsewhere.[19]

By integration of eq 10 or 11 with respect to z, a simple integral equation is obtained which describes the angular dependence of the fluorescence expected from a particular fluorescence density profile ($\rho(z)$)

$$F_{i,o}(\theta_{i,o};\rho(z)) = A\int_0^d Q(z)\ \rho(z)\ G_{i,o}(\theta_{i,o};z)\ dz \quad (12)$$

where d is the film thickness, as before. The pair of subscripts (i,o) indicate that eq 12 is actually two equations: one for incident angle variation and one for observation angle variation. The expressions $G_{i,o}$, which have both a distance (z) and angular ($\theta_{i,o}$) dependence, are known as the kernels of the equation. The parenthetical inclusion of the term ($\rho(z)$) on the left-hand side of eq 12 is meant to indicate that the shapes of the variable-angle fluorescence data curves ($F_{i,o}$) are partially determined by the shape of the fluorescence density profile ($\rho(z)$). The shapes of the data curves ($F_{i,o}$) are also partially determined by the shape of the quantum yield term ($Q(z)$). However, this is a relatively small effect for nonmetallic interfaces.

Under conditions in which the index of refraction of the bulk is the same as the index of the film, the kernels ($G_{i,o}$), in eq 12, have a z dependence only for "supercritical"[7] angles, i.e.; angles greater than the critical angle (θ_c) of the prism/film interface ($\theta_c = \sin^{-1}(n_p/n_b)$). At supercritical incident angles ($\theta_i > \theta_c$) an evanescent wave penetrates from the prism/film interface into the film (Figure 1e,f). At supercritical observation angles ($\theta_o > \theta_c$) the fluorescence observed emanates from evanescent components of the fluorophore emission. For a film which is index matched with the bulk material, information about the fluorescence density profile is only contained in the supercritical part of a variable-angle fluorescence data curve. In this case eq 12 can be written in the form of a Laplace transform,[13,14] and finding the fluorescence density profile from a fluorescence data curve is equivalent to performing an inverse Laplace transform.

More generally, the problem of obtaining the fluorescence density profile ($\rho(z)$) from the variable-angle fluorescence data curve ($F_{i,o}$) can be categorized as an "inverse problem".[22] Inverse problems are in general difficult to solve exactly, and one must in many cases be satisfied with obtaining various parameters of the solution. One characteristic of many inverse problems that makes them difficult to solve exactly is that they are unstable. Instability implies that unknown functions ($\rho(z)$) that differ widely can correspond to very similar variable-angle fluorescence data curves. One factor which contributes to instability is the limited domain for which the kernels $G_{i,o}$ are known.

Change in the Apparent Fluorescence Quantum Yield with Location. The expression "apparent (fluorescence) quantum yield" has been used to describe the theoretical dependence of observed fluorescence on distance of a fluorophore from a highly reflecting surface.[23] Dependence of the lifetime of fluorophores located close to a metal surface, on distance from that surface, was first observed by Drexhage.[24] A theoretical interpretation of this lifetime dependence that quantitatively describes the data is available.[23,25] This theoretical interpretation predicts that lifetimes will have a dependence upon distance from any interface which reflects a part of the emitted radiation. The lifetimes are equated to the inverse of the total power dissipated from an oscillating dipole emitter. The magnitude of this dependence is related to the magnitude of the reflection coefficient of the interface, such that the effect is less for dielectric interfaces than for metal/dielectric interfaces.

The model for a fluorophore as a constant-power dipole[7] predicts that the total power dissipated by a constantly illuminated fluorophore in the presence of a reflecting interface should have no functionality with respect to distance from that interface. One consequence is that theoretical estimates of fluorescence based upon the model of a fluorophore as an oscillating dipole should be modified by normalizing to total power dissipated by that dipole.[7,11] In terms of our notation, the effect is that the term $Q(z)$, which first appears in eq 9, would have a dependence on z which can be predicted theoretically. By solving the inverse problem (eq 12) completely one would obtain the product $Q(z)\rho(z)$ instead of $\rho(z)$. The functionality of $Q(z)$ can be determined by a numerical integration. The predicted change in Q with respect to z is relatively small for dielectric interfaces. For a sapphire/L-B film/air interface, where the film is 55.44 nm thick, Q increases by about 12% as one traverses the film from the prism/film interface to the film/air interface.[19] It should be mentioned that the precise functionality of the apparent quantum yield ($Q(z)$) has not been verified experimentally and that at least one conflicting theory exists.[26] The consequences of the possible functionality of Q with respect to z are discussed later in reference to the results.

Experimental Section

Apparatus. Figure 3 illustrates the central components of the apparatus. An argon ion laser provided the excitation light (λ_i = 488 nm). The laser was oriented so that the emitted light was perpendicularly polarized (TE) with respect to the plane of incidence. Incident angle variation within the illuminated area was minimized by focusing the laser beam on the focal plane of the sapphire hemicylindrical prism (Insaco). The focal plane refers to a cylindrical surface a distance f from the curved surface of

(22) Parker, R. L. *Annu. Rev. Earth Planet. Sci.* **1977**, *5*, 35.
(23) Chance, R. R.; Prock, A.; Silbey, R.; *Adv. Chem. Phys.* **1978**, *37*, 1.
(24) Bucher, H.; Drexhage, K. H.; Fleck, M.; Kuhn, H.; Mobius, D.; Schafer, F. P.; Sodermann, J.; Sperling, W.; Tillmann, P.; Wiegand, J. *Mol. Cryst.* **1967**, *2*, 199.
(25) Ford, G. W.; Weber, W. H. *Phys. Rep.* **1984**, *113*, 195.
(26) Deri, R. J. *Chem. Phys. Lett.* **1983**, *98*, 485.

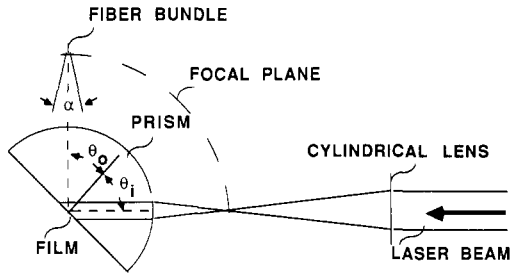

Figure 3. Two-dimensional view of apparatus used to collect fluorescence. The numerical aperture of the fiber bundle is indicated by the symbol α. Definition of the focal plane is given in the text.

the prism, defined by $f = [n_p/(n_p - 1)]R$, where R is the prism radius. Sapphire is uniaxially birefringent. The optical axis of the sapphire prism was oriented along the axis of the hemicylinder (by specific request). Propagation of the perpendicular polarized (TE) light inside the prism can be described by using only the extraordinary refractive index. This refractive index was interpolated from published values[27,28] as 1.768 at 488 nm and 1.766 at 510 nm. The laser power was 500 mW, which was attenuated to approximately 70 mW by neutral density filters. A modified X-ray diffraction goniometer (Rigaku) was employed to rotate the prism with respect to the incident laser beam, thus varying the incident angle, and to rotate the detector around the prism, thus varying the observation angle. At the fastest possible rotation rate (4°/min) a scan through 90° (grazing to normal) took 22.5 min. All scans for data presented in this paper were begun at 90° (grazing) and terminated at 0° (normal). The fluorescence was detected by a fiber bundle arranged in a rectangular array (0.5 mm × 3.9 mm; acceptance angle 15°) contained within a wedge-shaped holder to deflect the reflected laser beam. A film polarizer restricted the fluorescence collected to the perpendicular polarized component. An error of 0.5% was estimated in this detected polarization state (i.e., 0.5% of the detected light was TM polarized). The detector was placed on the focal plane of the prism to minimize observation angle variation at one detector position. Fluorescence collected by the fiber was spectrally analyzed by an Hr-640 optical spectrometer (Instruments, S.A.); current pulses produced by individual photons in a Hamamatsu PMT were amplified, discriminated, and digitized by Ortec photon-counting equipment and sent directly to a Charles River data system for storage. For collection of variable-angle fluorescence data the fiber bundle output was filtered by a 488-nm blocking interference filter (Pomfret) before it entered the optical spectrometer.

For fixed observation angle experiments, the alignment procedure was such that the angle of the detector was fixed roughly (mechanically) by eye, and then optical methods were used to center the incident beam on the prism and calibrate the scale so that 0° corresponded to normal incidence. The outcome of this alignment procedure, in terms of experimental results, is that fixed observation angles vary between 60° and 70° among experiments. The alignment procedure resulted from the use of a modified X-ray diffraction goniometer as an experimental apparatus that was not originally designed to accommodate fixed observation angle experiments. (The details of alignment procedures and design are described in detail elsewhere.[19])

Langmuir–Blodgett Deposition. Langmuir-Blodgett (L–B) deposition has been described in detail elsewhere.[17] A specially designed Teflon holder allowed deposition directly onto the flat surface of the hemicylindrical sapphire prism, while leaving the curved surfaces and the ends free of any film. The two molecules used to fabricate the thin films were cadmium arachidate (CdC_{20}) and *N,N'*-dioctadecyloxacarbocyanine *p*-toluenesulfonate (a cyanine dye obtained from Eastman Kodac). The cyanine dye (Figure 4) has an absorption maximum at 495 nm and a bimodal fluorescence emission pattern that has been presented elsewhere.[16]

(27) Wolf, W. L. In *Handbook of Optics*; Driscoll, W. G., Vaughan, W., Eds.; McGraw Hill: New York, 1978; Vol. 7, p 101.
(28) Bennett, J. M.; Bennett, H. E. In *Handbook of Optics*; Driscoll, W. G., Vaughan, W., Eds.; McGraw Hill: New York, 1978; Vol. 10, p 106.

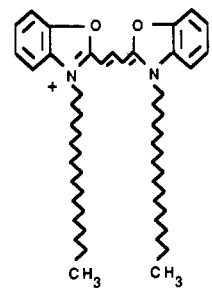

Figure 4. Line structure of cyanine dye.

Table I. Summary of Experimental Categories and Film Types

category	interface	data curve type
1	prism/film/air	variable incident angle
2	prism/film/fluid	variable incident angle
3	prism/film/air	variable observation angle
4	prism/film/fluid	variable observation angle
film type		range, nm
I		0–52.80
II		0–15.84
III		47.52–52.80

For deposition of the dye, the dye was incorporated into a CdC_{20} matrix at a 1:10 molar ratio (1 dye:10 acid). Both the acid and acid–dye mixtures were diluted in spectral grade methylene chloride for application to the subphase, which was 5×10^{-4} M cadmium chloride. Deposition onto the prism was carried out at a film pressure of 40 dyn/cm^2. Films were allowed to dry approximately 16 h before fluorescence data were collected. The ordinary refractive index of monolayer assemblies fabricated from CdC_{20} and a cyanine dye has been determined to be 1.526 for λ = 526 nm, and the thickness of a single CdC_{20} monolayer has been determined as 2.64 nm.[17] The dye fluorophore emission dipoles are thought to be confined to planes parallel to the film plane.[17] We do not have data on the refractive index dispersion of the L–B films.

Index Matching Fluid. An attempt was made to find a fluid that exactly matched the refractive index of the film, without disrupting the monolayers. Commercially available index matching solutions (Cargille) with the appropriate refractive index were readily available but were found to disrupt the monolayers. It was found, after some experimentation, that only polar fluids (with as much polarity as water) would leave the layers intact. We chose to use saturated potassium iodide (n_b = 1.475). The fluid was contained in a chamber made from a silastic gasket (3 mm thick) backed with a glass slide pressed to the flat surface of the prism by using a black anodized aluminum backing plate.

Results

Two types of fluorescence measurements were made. In order to obtain a variable incident angle fluorescence data curve fluorescence measurements were made at a fixed observation angle (with respect to a normal to the interface) for incident angles which ranged from grazing angle (90°) to normal (0°). To obtain a variable observation angle fluorescence data curve, the incident angle was held fixed and fluorescence was collected for observation angles in this same range. Both variable incident and variable observation angle fluorescence data curves were obtained from each of two interface configurations: prism/film/air and prism/film/high-index fluid. The fluid was chosen so that it would have an index close to that of the film. In addition to having the appropriate index the fluid had to be nondisruptive to the layer structure of the film (see Experimental Section). The four experimental categories are summarized in Table I. Each category of experiment was performed on each of three film types constructed in the L–B trough. The film types were all 55.44 nm thick but differed with respect to the range (in terms of distance

Table II. Fit of Parameters[a] of Rectangular Model to Discrete Model

		film type I (0–52.80 nm)			film type II (0–15.84 nm)			film type III (42.24–52.80 nm)		
interface	$Q(z)$	position	width	av[b]	position	width	av	position	width	av
				Three-Parameter Fit						
prism/film/air	calc	28.38[c]	56.08	0.0025	9.12	18.93	0.0024	47.61	15.53	0.0026
	comp	27.67	55.71	0.0024	9.05	18.94	0.0024	47.52	14.93	0.0024
prism/film/fluid	calc	28.04	55.62	0.0025	9.13	18.63	0.0025	47.56	16.16	0.0026
	comp	27.66	55.66	0.0025	8.99	18.74	0.0025	47.62	15.87	0.0025
				Two-Parameter Fit						
prism/flim/air	calc	25.96		0.0297	8.92		0.0068	47.37		0.0039
	comp	25.30		0.0258	8.84		0.0068	47.29		0.0039
prism/film/fluid	calc	25.77		0.0097	8.87		0.0035	47.37		0.0029
	comp	25.40		0.0097	8.79		0.0035	47.36		0.0029

[a] Amplitude values not included (see text). [b] Average fractional difference between curves. [c] Units for position and width are nanometers.

from the prism/film interface) in which the planes of fluorophores were contained (see Table I). Fluorescence was excited at 488 nm and was collected at 510 nm in order to obtain all variable-angle data curves presented below.

The film types were modeled in terms of a fluorescence density profile, which will be referred to as rectangular (Figure 2). Ideal rectangular profiles can be described completely by three parameters: an amplitude, a position, and a width. The equation used to generate a data curve from an ideal rectangular profile is obtained by integrating eq 12 over limits determined by the position and width. It is assumed that the fluorescence density is constant over these limits. It has also been assumed that the quantum yield term ($Q(z)$) is constant over the range of the rectangular profile. The resulting expression is

$$F_{i,o}(\theta_{i,o};A,z_0,w) = A\int_{z_0-w/2}^{z_0+w/2} G_{i,o}(\theta_{i,o},z)\,dz \qquad (13)$$

where the parameters of the amplitude (A), position or center (z_0), and width (w) have been included parenthetically on the left-hand side of eq 13 in order to indicate that they influence the shape of the variable-angle fluorescence data curves ($F_{i,o}$). As with eq 12, the pair of subscripts (i,o) indicate that eq 13 represents two equations: one for incident angle variation and one for observation angle variation. All terms with neither an angular ($\theta_{i,o}$) nor a distance (z) dependence have been subsumed in the amplitude term.

Theoretical data curves generated by a rectangular profile can be fit quite accurately with a simpler representation involving only two parameters: an amplitude and an approximate position. This simpler representation results in a correspondingly simpler expression for the variable-angle fluorescence data curve.

$$F_{i,o}(\theta_{i,o};A,z_0) = A\,G_{i,o}(\theta_{i,o},z_0) \qquad (14)$$

The best fit of the position parameter (z_0), which appears in eq 14, gives an approximate location of the center of the rectangular profile. The shapes of the data curves generated from this simpler representation are very similar to the data curves generated by an actual rectangular profile centered at approximately z_0, if amplitude is adjusted accordingly. In fact, there is a family of rectangular profiles which all generate very similar fluorescence data curves if amplitude is adjusted to obtain a best fit. This family consists of all the rectangular profiles with approximately the same position (or center) (Figure 5). In the limit (as the width approaches zero) one obtains a "rectangular profile" that can be represented with only position (eq 14). The similarity of data curves produced by this family of profiles is an example of the instability of the inverse problem under the conditions of an arbitrary amplitude.

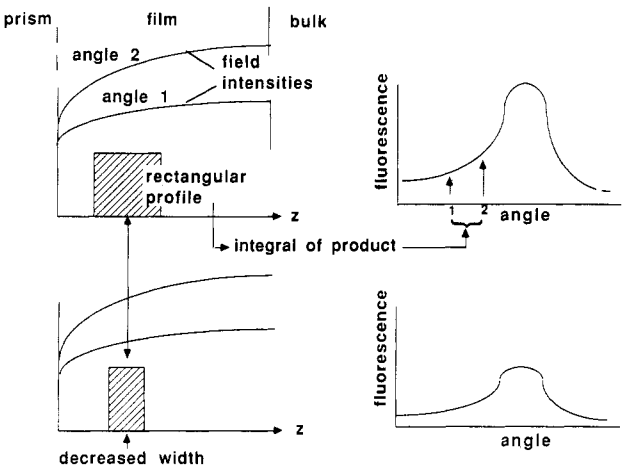

Figure 5. Variable-angle fluorescence data curves produced by a family of rectangular profiles have very similar shapes when amplitude is adjusted accordingly. This family consists of rectangular profiles with the same approximate position (or center).

Modeling with Simulated Data. Since each fluorophore is contained in a discrete plane, profiles constructed by the L–B method can be represented more precisely as discrete functions with a spacing of 5.28 nm between values than as rectangular profiles having a uniform distribution of fluorophores throughout a particular range. The model of a rectangular profile (Figure 2) was chosen because it has more general application than a discrete representation since profiles of biomedical interest would not usually be made up of discrete layers. Another advantage of using this model is that it results in analytical expressions for theoretical data curves (and also for the derivatives of these expressions with respect to each parameter) which are relatively simple. This advantage is lost unless the quantum yield function ($Q(z)$) is approximated as a constant. Simulated data curves generated from discrete profiles representing each film type can be fit with a great degree of accuracy by using, as a model, a rectangular profile with the appropriate position and width. The inclusion of the theoretical dependence of the quantum yield on distance (z) has only a small effect on the values obtained for these parameters.

In Table II (three-parameter fit) is listed the best fit of position and width (using eq 13) of an ideal rectangular profile to data generated from the discrete representations of each film type. Discrete representations were obtained by summing the energy available for fluorescence (given by eq 10 or 11) at each distance from the prism/film interface where a fluorophore plane appeared in a particular film. (The fluorophore containing planes adjacent to the prism/film interface in film types I and II was assumed to produce half the fluorescence of other planes since they

contain half the concentration of fluorophores.) Parameters were fit to each data set by a least-squares criterion: the smallest sum of squares of differences between data points and the theoretical curve. Parameter fits are listed for each of two interface configurations: prism/film/air and prism/film/high-index fluid. The data curves obtained from the rectangular profile fit are quite close to the data curves generated from the more precise discrete model (less than 0.3% average difference). Simulated variable incident and observation angle data curves produced identical results. In general the best fit of the parameter of width is greater than that implied by the actual range in which the fluorescent planes of the discrete profiles are contained (Table I). The best fit of the position parameter (or center) is also slightly greater than the actual position of the center of this range. Table II essentially displays the effect on the position and width determinations of adopting a model in which the fluorophore distribution is uniform throughout a particular range, instead of being confined to discrete planes.

Table II also includes a comparison of position and width determinations, which result from the case in which the quantum yield function ($Q(z)$) is constant throughout the film versus the case in which it has the functionality specified by ref 7 and 25. In the second column of Table II, under the heading $Q(z)$, appear the abbreviations comp or const: comp indicates that $Q(z)$ was computed as prescribed by ref 7 and 25 in order to obtain the generated data from the discrete representation via eq 10; const indicates that $Q(z)$ was assumed to be constant in order to obtain the generated data. Position and width estimates obtained for the computed $Q(z)$ and the constant $Q(z)$ are all within 1 nm. These simulated results reveal that the theoretical functionality of $Q(z)$ has only a slight effect on the estimates of position and width of a rectangular profile.

Note that the amplitude values have been deleted in Table II. In general, amplitude values are not included in the tables. Even though it is necessary to fit an amplitude parameter to each data set, its value in terms of the analysis is arbitrary, since no attempt was made to predict absolute values of fluorescence density or dye concentration.

In the bottom portion of Table II (two-parameter fit) are listed fits of a position parameter, obtained by using the simpler representation (eq 14), to the same simulated data curves generated from the precise discrete model. Note that the average fractional differences between the two-parameter fitting curve (eq 14) and the data curve generated from the discrete model are larger than those for the three-parameter fit but are still quite small. The effect of assuming that $Q(z)$ is constant throughout the film, on estimates of the position parameter obtained via eq 14, is less than 0.5 nm.

Results obtained by using simulated data revealed that fitting the simpler representation (eq 14) involving the two parameters of amplitude and position could be achieved with relative ease, while adding the third parameter of width to the model (eq 13) increased the difficulty substantially. A relatively simple Newtons method[29] was adequate to fit amplitude and position to data curves generated from the discrete model representing each film type. The method was rapid convergence and good accuracy (positional parameter within 0.5 nm of parameter with noise-free data) for signal to noise levels of up to 20:1 (300 points). (Noise was inserted into simulated data curves in the form of a random variable, normally distributed around each function value.)

Table III. Three-Parameter Fit to Simulated Noisy Data Curves from Film Type I

data set	position, nm	width, nm	χ^a
1	28.26	51.08	0.829
2	28.16	55.29	0.629
3	28.57	58.80	0.597
4	28.03	58.60	0.853
5	28.22	54.78	0.500
	$\bar{x}$ = 28.25	$\bar{x}$ = 55.71	
	SD = 0.198	SD = 3.17	

[a] Reduced χ^2.

Table IV. Summary of Two-Parameter Fits[a] to Actual Data

exptl category	film type I (0–52.80 nm) position	film type I χ^b	film type II (0–15.84 nm) position	film type II χ	film type III (42.24–52.8 nm) position	film type III χ
1	24.47[c]	2.31	5.54	0.81	45.39	1.41
2	20.11	7.57	4.16	4.14	42.19	12.19
3	24.38	11.54	8.44	1.33	43.05	4.59
4	16.21	5.16	6.24	3.44	53.95	9.47

[a] Amplitude values not included (see text). [b] Reduced χ^2. [c] Units for position are in nanometers.

In order to fit the more complete representation (eq 13) involving amplitude, position (or center), and width to simulated data, we needed to resort to a more sophisticated numerical technique known as the Marquardt method.[30] The method has relatively slow but steady convergence for signal to noise levels of up to 50:1 (300 points). Higher noise levels caused problems such as lack of convergence and dependence of estimates on initial guesses.

Table III presents a more detailed (empirical) noise analysis of data generated from the discrete representation ($Q(z)$-computed) for film type I into which noise was inserted. Noise was inserted into five data curves, which were generated from the discrete model, in the form of a random variable, normally distributed around each data point, with variance equal to the square root of the signal at each point. By inserting noise in this manner we attempted to mimic the quantum noise of photon collection. The scale of the data curves was chosen so that the magnitude of the values would correspond to numbers of photon counts obtained in actual experiments described in the next section. The interface configuration was prism/film/air. Table III essentially displays the variation in position and width estimates expected to result from the quantum noise of photon collection.

Data from L–B-Deposited Films. Table IV summarizes the results of a two-parameter fit (using eq 14) to data from each of the four experimental categories taken from each of the film types. Film types used to obtain data in each experimental category were made on the same occasion in the trough. Thus the differences in position estimates between experimental categories can be attributed to causes other than variation in L–B construction of the film types. Table II (two-parameter fit) lists position estimates which would be obtained under ideal conditions based on the discrete model with no noise inserted. Figures 6–9 (parts a–c) display the data curves from the four categories of experiments together with the theoretical curve obtained from a two-parameter fit. In Figures 6–9 (part d) are displayed the theoretical curves obtained from the precise discrete representation of each film type. For

(29) Rice, J. R. *Numerical Methods, Software, and Analysis*; McGraw Hill: New York, 1[illegible] p 239.

(30) Press, W. H.; Flannery, B. P.; Teukolsky, S. A.; Vetterling, W. T. *Numerical Recipes*; Cambridge University Press: New York, 1986; p 523.

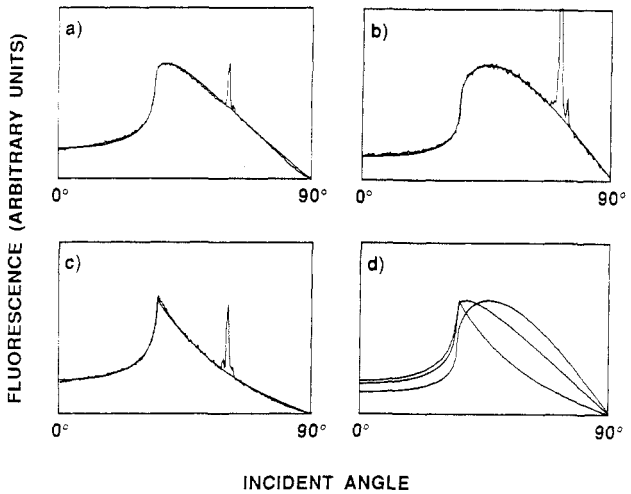

Figure 6. Two-parameter fits: (a–c) Data curves in experimental category 1 displayed together with the best fit obtained from eq 14. (d) Ideal theoretical data curves for each film type, obtained from the discrete model, are displayed together. See Table I for description of film types and definition of experimental categories; see Table IV for summary of position determinations.

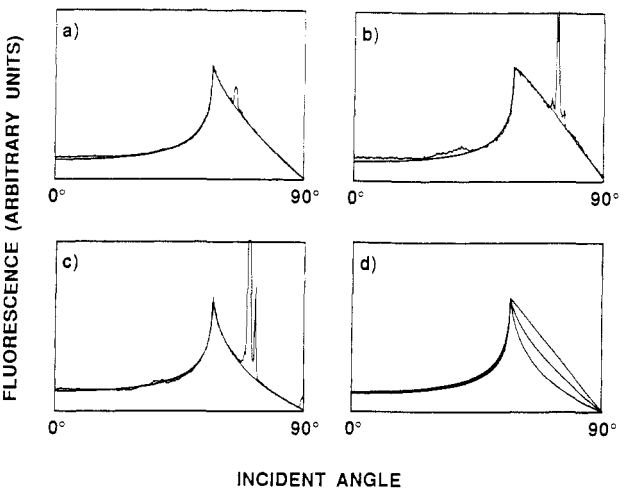

Figure 7. Two-parameter fits: (a–c) Data curves in experimental category 2 displayed together with the best fit obtained from eq 14. (d) Ideal theoretical data curves for each film type, obtained from the discrete model, are displayed together. See Table I for description of film types and definition of experimental categories; see Table IV for summary of position determinations.

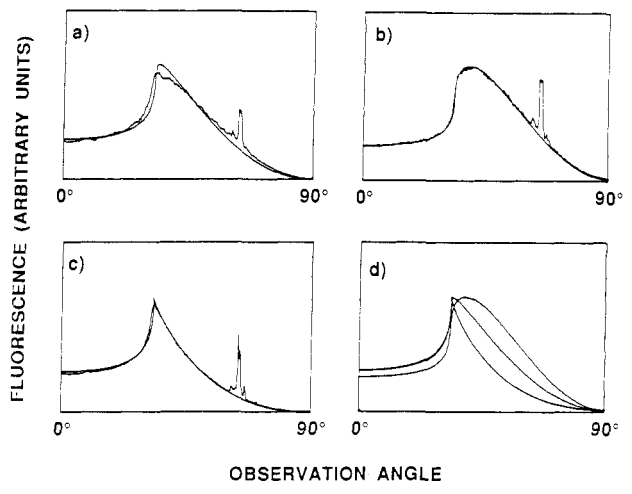

Figure 8. Two-parameter fits: (a–c) Data curves in experimental category 3 displayed together with the best fit obtained from eq 14. (d) Ideal theoretical data curves for each film type, obtained from the discrete model, are displayed together. See Table I for description of film types and definition of experimental categories; see Table IV for summary of position determinations.

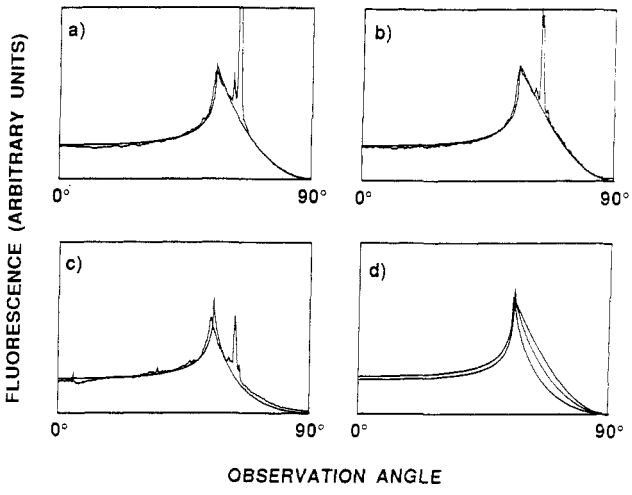

Figure 9. Two-parameter fits: (a–c) Data curves in experimental category 4 displayed together with the best fit obtained from eq 14. (d) Ideal theoretical data curves for each film type, obtained from the discrete model, are displayed together. See Table I for description of film types and definition of experimental categories; see Table IV for summary of position determinations.

presentation purposes the scale of the ordinate was adjusted in each figure so that the maximums of fluorescence values would coincide for each of the curves. Regarding Figures 6–9 (a–c) one can see that a peak in the fluorescence values exists in the experimental data curves at the fixed incident or observation angle used in each of the experiments. This is because in order to obtain the variable angle data the detector must scan through the laser beam, which reflects from the prism/film interface. Some of this directly reflected laser light shows up in the variable angle data. Data points which were obviously a result of this directly reflected light were deleted from the data sets before applying the numerical analysis. This same deletion was performed on all data sets described below.

Values of the extraordinary refractive index of the sapphire prism for perpendicular polarized light at 488 at 510 nm were interpolated from published values as described in the Experimental Section. The angle (θ_c) at which the sharp peak (excluding the laser line) occurs in data obtained for film type III and interface configuration prism/film/air (Figures 6c and 8c) is indicative of the relative refractive index of the prism and air ($n_p = n_a/\sin \theta_c$). Similarly, the angle at which the sharp peaks occur in data curves from all the film types for the prism/film/high-index fluid interface configuration (experimental categories 2 and 4) is indicative of the relative refractive index of the prism and the fluid. For experimental categories 1 and 2 (variable incident angle data curves) the refractive index of the sapphire prism obtained from the angles at which the sharp peak occurs (as described above) agrees with those interpolated from published values. For experimental categories 3 and 4 (variable observation angle data curves) the refractive index of the sapphire prism obtained from the angles at which this sharp peak occurs in the variable angle data curve was 1.853 and 1.801, respectively. These values are considerably higher than expected. The best fits of theoretical curves to variable observation angle data curves from all film types were obtained by consistently using these values.

Errors in observation angle are discussed elsewhere for this particular apparatus.[16,19] For observation angles greater than 20° the error bar width in the angle is about

Table V. Comparison of Three- and Two-Parameter Fits to Actual Data from Film Type I (0–52.80 nm)

data set	three-parameter fit[a] position	width	χ^b	two-parameter fit position	χ
1	24.60[c]	14	2.27	24.47	2.31
2	23.71	10	2.64	22.56	2.59
3	22.24	2	3.82	22.23	3.79
4	27.23	55	1.80	24.99	2.68
5	22.33	6	5.21	22.23	5.11
	$\bar{x}$, 24.02 SD = 2.04	$\bar{x}$ = 17 SD = 21			

[a] Amplitude values not included (see text). [b] Reduced χ^2. [c] Units for position and width are in nanometers.

1.3° ($\theta_0 \pm 0.65°$). The variation in observation angle at each detector position has a smoothing effect on the experimental curve. An analysis of this smoothing effect has not been included in the theoretical curves.

Our experience with simulated data indicated that a two-parameter fit (amplitude and width) could be obtained with relative ease, while the difficulty of fitting parameters was increased considerably when a width was added to the first two parameters. The reason for this increased difficulty of fitting the third parameter is basically that theoretical data curves of rectangular profiles with the same position, but different widths, are of nearly identical shape once the amplitudes have been adjusted accordingly.

An attempt to fit a width parameter to data from experimental category 1 illustrates the difficulties involved with actual data. Experimental category 1, together with film type I, was expected to have the most chance of producing a reasonable estimate of width for a number of reasons. Firstly, the theoretical development that forms the basis for predicting the energy distribution within the film for incident angle variation is more simple and straightforward than that which predicts the angular distribution of fluorescence observed (at fixed incident angle), which leaves less room for overlooking a theoretically important variable in the analysis. Secondly, for the prism/film/air interface configuration, data points in the entire angular range (0–90°) contain profile information. This increases the domain of the kernel (G) which appears in eq 12 and reduces the instability of the inverse problem. Thirdly, the polarization of the incident beam is that of the light coming from the laser and therefore is less likely to be contaminated with other components. Finally, the theoretical curves used as a model for film type I are most different in shape from curves obtained from the representation involving only two parameters, since the width of this rectangular profile is the greatest.

Five different variable incident angle fluorescence data curves from a prism/film/air interface configuration and film type I (Table I) were analyzed in terms of the more complete representation (eq 13), involving the three parameters of amplitude, position, and width. In Table V values of the best fits of the parameters of position and width are tabulated for these five data curves. Three of the data curves (data sets 1–3) were taken repeatedly from one film. The other two curves (data sets 4 and 5) were taken from films (of type I) which were made on two separate occasions. The values for width are all integers as a result of the numerical method used to obtain the best fit. A reduced χ^2 was calculated for each fit by assuming that the variance at each data point was equal to the square root of the signal (photon counts). χ^2 values obtained from a two-parameter fit (eq 14) are included for comparison. The χ^2 value should converge to 1.0 for fits

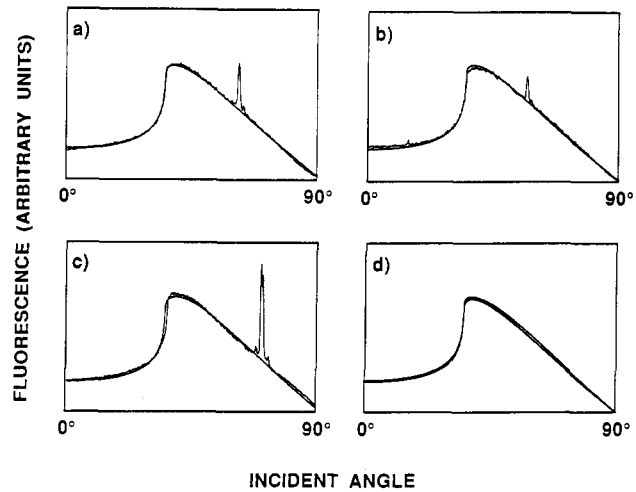

Figure 10. Three-parameter fits: (a–c) Data curves from film type I, experimental category 1 displayed together with the best fit obtained from eq 13. (d) Best fits are displayed together. See Table I for description of film types and definition of experimental categories; see Table V for summary of position and width determinations.

of theory to data which are consistent with hypothesis. Note that, in general, χ^2 values listed in Table IV for a two-parameter fit are of nearly the same magnitude as, or in some cases smaller than, the values for a three-parameter fit. This finding, taken together with the spread in the values of estimates of width as well as the deviation of the mean value of the widths from the true value, was interpreted as indicating that the data did not support a three-parameter fit. A comparison of values for width and position obtained from actual films (Table V) with those obtained from simulated data with equivalent noise levels (Table III) indicates that actual data curves contain some distortion as well as the quantum noise inherent to photon collection.

Since film I is made up completely of planes which contain fluorophores, it might be expected to absorb a significant amount of the incident radiation. To see if this effect was significant, the imaginary part of the refractive index of monolayers of the dye–arachidate matrix was estimated. By assuming that the extinction coefficient of the dye in the lattice was the same as that of the dye in solution a value of 4 (10^{-5}) for the imaginary part of the complex refractive index was obtained. In terms of a three-parameter fit to data curves this value is insignificant.

Figure 10a–c displays the variable incident angle fluorescence data curves from data sets 1, 2, and 3 of Table V, together with the theoretical curves obtained from the three-parameter (amplitude, position, and width) fit. The theoretical curves for best fits to each of the data curves are also displayed in order to demonstrate their similar shapes (Figure 10d). For presentation purposes the scale of the ordinate was adjusted in each figure so that the maximums of fluorescence values would coincide for each of the curves.

Discussion

General Discussion. Many dielectric films of biomedical interest are on the order of 10–20 nm thick. By using the method of L–B deposition fluorescence density profiles have been constructed in films which have a comparable thickness (55.44 nm). The L–B films used in this study had to be thick enough to permit a variety of approximate rectangular profiles of different widths to be constructed from the inherent integral layer structure

which restricts the distance between planes of fluorophores to a minimum of 5.28 nm.

The refractive index of the L–B films used in experiments described here (1.526) is considerably larger than that of most biopolymers of interest (~1.3–1.4). However, the relative refractive index for a sapphire/L–B film interface (1.16) is of approximately the same magnitude as that of a quartz or glass/water interface (~1.10), which is the most common interface used for evanescent wave spectroscopy of biopolymers.[4,5] For supercritical angles the domain over which the kernel G in eq 12 is known is determined by the magnitude of this relative refractive index. As the relative refractive index increases this domain becomes greater. An infinite domain would be ideal. The limited size of the domain over which the kernel G is known contributes to the instability of the inverse problem.

Biopolymers would form films with distinct fluorescence density profiles if fluorophores were located in distinct moieties and the molecule had an orientational preference on a surface. These profiles would undoubtedly not be rectangular. However, the parameters found by using a rectangular model could indicate the shape of the actual profile. This statement can be justified by examples.[19]

An exact solution to the inverse problem (eq 12) would result in a complete description to the fluorescence density profile. It can be shown mathematically that, if one is limited to discrete data values (which is always the case), the inverse problem does not produce a unique solution.[22] However, it is not this lack of theoretical uniqueness which is, from a practical point of view, the greatest obstacle to finding an exact solution. Different profiles of interest will, in general, produce simulated data curves which are distinguishable to some degree. An exact solution is difficult to obtain from real data because the degree to which data curves from different profiles differ can be miniscule, even though the profiles have quite different shapes. This characteristic of the inverse problem is called instability, and its definition is somewhat more vague than that of nonuniqueness.

One approach for dealing with the instability of the inverse problem is to restrict the solution to a class of possible functions, or, in other words, make a model of the solution and vary parameters of that model to obtain a best fit. Here the original model was a rectangular profile. Although, with simulated results, reasonable estimates of all three parameters (amplitude, position, and width) could be obtained, the actual data (results presented in Table V and Figure 10) did not support this three-parameter fit. It was concluded that the data curves contain some distortion, as well as the quantum noise inherent to photon collection. It might be that a more sophisticated statistical analysis of a larger sample of data curves would produce a reasonable width estimate.

In an experiment in which the absolute quantity of fluorophores could be correlated with the number of photon counts, rectangular profiles with different widths would be easily distinguishable by their distinct amplitudes. Unfortunately, the number of photon counts can vary with so many factors in an actual experiment (quantum yield, excitation source power, collection efficiency, etc.) that the relation between photon counts and absolute quantity of fluorophores is rarely known in fluorescence spectroscopies. Therefore, one is forced to treat the amplitude of profiles as an arbitrary parameter, i.e., as a factor uncorrelated to the profile's shape.

In terms of the analysis of variable-angle fluorescence data curves obtainable on our present apparatus, rectangular profiles look very similar to one plane of fluorophores. The position of this plane (in terms of distance from the prism/film interface) indicates the position (or approximate center) of the rectangular profile. In more general terms, profiles which are grouped around some location will "look" very similar to an imaginary plane of fluorophores located at a position which is indicative of the location of the distribution.

The position parameter alone would be useful information about a film if other characteristics of the film were known. For example, the fluorophore thickness of a film could be deduced as being equal to about twice the position parameter if fluorophores were known to be uniformly distributed in the film. Alternatively, a position parameter located near one interface of a film, whose thickness had been determined by other methods, would indicate a preferential orientation of the constituents of the film.

Experimental Errors and Possible Improvements. Table IV summarizes the two-parameter fit for the four experimental categories listed in Table I. The same films were used to obtain data curves in each category for each of the film types. For reasons outlined in the Results section, data curves obtained in experimental category 1 (variable incident angle; prism/film/air interface configuration) are probably most reliable. The relatively close correspondence of position determinations for category 1 (Table IV) with those expected on the basis of the theoretical modeling (Table II) give confidence that each of the film types was constructed properly.

One can make two generalizations on the basis of results presented in Table IV. Firstly, considering the prism/film/air interface configuration, position estimates obtained from variable observation angle data curves (experimental category 3, Table I) are less reliable, judging from the larger reduced χ^2 values, than those obtained from incident angle variation (experimental category 1, Table I). Oddly enough, this does not seem to result in less accurate position determinations. Secondly, the position estimates are less accurate for the prism/film/high-index fluid interface configuration (experimental categories 2 and 4) than for the prism/film/air interface configuration (experimental categories 1 and 3). This is especially apparent for determinations of position of film type I. In nearly all cases where inaccuracies appear, the position appears to be underestimated.

Position estimates obtained from variable observation angle data curves (experimental category 3, Table I) may be less reliable than those obtained from their incident angle counterparts (experimental category 1) simply because of a greater error in the detected polarization. As mentioned in the Experimental Section, the detected fluorescence emission was restricted to the TE polarization by a filter polarizer, with the error in the polarization state being about 0.5%.

Besides improving the quality of the detection polarizers, one might obtain less distorted variable observation angle data curves by using a different design. Our design was intended to minimize observation angle variation by collecting fluorescence at the focal point of the hemicylindrical prism. The advantage of using a fiber bundle for this purpose is that detected fluorescence can be restricted to radiation which converges on this focal plane by simply locating the surface of the fiber bundle at this plane. The cone of acceptance of detection is also easy to determine from the numerical aperture. The errors in observation angle result from the finite surface area of the fiber bundle. An alternate approach to this design is to use a lens with a circular aperture to collect the data. For this design

equations which completely describe the expected angular functionality of fluorescence have been derived.[7]

The lack of correspondence between the position determinations obtained from the prism/film/fluid interface, with those obtained from the prism/film/air interface, can be accounted for in a number of ways. It is possible that the film/fluid interface contains more distortions than the film/air interface. This might cause light scattering from this interface and modify the intensity distribution in the film. The presence of the fluid may also be distorting the lattice structure of the film. However, if the film is distorted by the presence of the fluid, this distortion appears to be completely reversible: if the film is washed and allowed to dry, the shape of the original variable incident angle fluorescence data curve, obtained for a film/prism/air interface configuration, is restored.[19]

As mentioned in the Results section, closer fits of the theoretical curves to the variable observation angle data curves were obtained if the index of the sapphire prism was assumed to be substantially higher than its value as interpolated from published data. The data from the various film types are internally consistent in this respect. For the prism/film/air interface configuration the sapphire index was indicated to be 1.853, and for the prism/film/high-index fluid interface configuration a value of 1.8006 was indicated. The estimation of the refractive index, using interpolation from published data, indicated a value of 1.766. This estimate incorporated the effects of refractive index dispersion and birefringence of the sapphire prism. The imaginary part of the refractive index of sapphire at both 488 and 510 nm, as indicated by its transmission properties,[31] is negligible. The hemicylindrical prism is slightly out of round; however, this slight distortion would be expected to affect both the variable incident and variable observation angle data curves to the same degree. Therefore we are at a loss to explain this anomaly.

Variable incident angle fluorescence data curves obtained with the prism/film/air interface configuration (experimental category 1, Table I) produced the best estimates of position if both accuracy and χ^2 values are taken into account. However, even these data curves contain some distortion, as well as the quantum noise inherent to photon collection. This is revealed most clearly by the failure of the analysis of these data curves to predict the width parameter of film type I. The distortion in the data curves could be caused by various factors including photobleaching of the sample, laser power fluctuations during data collection, small misalignments, or imperfect optical components. Of these factors, the effect of photobleaching during the relatively long data collection process (22.5 min) is of primary concern. This effect is difficult to quantify separately since the illumination of the sample is changing while an incident angle data curve is being taken. There are a number of reasons for discounting photobleaching as a huge effect. First, the relatively flat tails of the data curves for small incident angles (Figure 6) do not sink significantly below the theoretical curves as the angle approaches the normal. (Data points were taken from grazing angle to normal as described in the Experimental Section.) Secondly, data curves taken from grazing to normal appear to be the same shape as those taken in the reverse angular order.[19] Third, data curves taken repeatedly from the same area on the same film have approximately the same shape and amplitude.[19] For these reasons we do not believe the effect of photobleaching is greatly significant in the position determinations displayed in Table IV. However, this effect may well account for the variation and inaccuracies in the width determinations displayed in Table V, since the estimation of this parameter is very sensitive to slight distortions in the data curve.

In the last theoretical section the consequences of the model of a fluorophore as a constant-power dipole were briefly outlined. The net effect of this model is that by solving the inverse problem completely one would be obtaining a fluorescence density profile ($\rho(z)$) weighted by another function ($Q(z)$) which has the effect of a quantum yield. The function $Q(z)$ can be derived for our specific experimental conditions by employing numerical methods.[7,25] The inclusion of the $Q(z)$ functionality in our analysis would not drastically affect the accuracy of the width determinations of film type I, which are listed in Table V. One might expect each width estimate to be altered by about 1 nm (see Table II, column two). If the distortion in fluorescence data curves could be reduced, then variable-angle fluorescence data curves from films containing successive layers of fluorophores (such as film type I) would be ideal for experimentally verifying that $Q(z)$ conforms to theoretical expectation, since in this case the fluorescence density profile ($\rho(z)$) is essentially a constant.

Conclusion

Variable-angle fluorescence data curves can provide useful information about fluorescence density profiles of dielectric films. Information which can be obtained from real data curves is limited by various interactive theoretical and experimental factors including the instability of the inverse problem, the noise inherent to photon collection, and the distortion of data curves caused by nonideal experimental conditions. With our apparatus, information about rectangular fluorescence density profiles of thin films, which are of a thickness and prism/film relative refractive index comparable to films of biomedical interest, is limited to estimation of an approximate position of the profile. This position parameter could be used to deduce a fluorescence layer thickness or orientational preference of an interfacial biopolymer film if other characteristics of the film were known.

Acknowledgment. This project was funded by a University of Utah Research Committee graduate research fellowship (P. A. Suci), by a grant from the Whitaker Foundation, by NIH Grant HL 32132, and by the Center for Biopolymers at Interfaces at the University of Utah.

Registry No. CdC_{20}, 14923-81-0; *N,N'*-dioctadecyloxacarbocyanine *p*-toluenesulfonate, 60711-74-2.

(31) Wolf, W. L. In *Handbook of Optics*; Driscoll, W. G., Vaughan, W., Eds.; McGraw Hill: New York, 1978; Vol. 7, p 23.